

UNSTEADY FLOW OVER A SD7003 AIRFOIL AT LOW REYNOLDS NUMBERS USING A HIGH-ORDER ACCURATE FLUX RECONSTRUCTION SCHEME

Vilem Skarolek* , Koji Miyaji**

*Graduate School of Environment and Information Sciences, **Department of Ocean and Space System Engineering, Yokohama National University, Yokohama, Japan
skarolek-vilem-yf@ynu.jp, miyaji@ynu.jp

Keywords: *flux reconstruction, large-eddy simulations (LES), laminar separation bubble (LSB), viscous flows, transition to turbulence*

Abstract

Implicit large-eddy simulations (ILES) of transitional separated flow were performed using a high-order flux reconstruction (FR) scheme on the configuration of SD7003 wing section at low-Reynolds number $Re = 60,000$ for which complex transitional flow dominates the flow field on the upper surface of the wing. Presented study is an attempt to assess the performance and suitability of the FR scheme for accurate simulations of transitional flow with small (grid-scale) vortices. Simulations are carried out with polynomial degree $p = 2$ (3rd-order) and $p = 3$ (4th-order) resulting in up to 2,000,000 degrees of freedom. Second order simulations has been included, dependency of the grid and angle of attack (4° & 8°) were surveyed to improve fidelity of simulations.

1 Introduction

Increasing performance of current computers allows to simulate flow problems of higher complexity with more matured and sophisticated numerical methods than it was possible ever before. In the last two decades, computational fluid dynamics (CFD) simulations have become necessary part of the design process in majority of engineering fields. Mostly lower fidelity methods are being used and since lower fidelity methods do not take into account phenomena that are im-

portant for some design work (e.g. vortex dominated flows, sonic boom, aero-acoustics and noise etc.) development of high fidelity tools which are reliable and easy to use is necessary.

Recent advances in miniaturization accelerates development of micro-air vehicles (MAVs) which usually work in the regime of low Reynolds (Re) numbers about $10^4 \sim 10^5$. Let's mention also other applications such as propellers, leading-edge control devices, wind turbines, high-altitude aircrafts for which their operation can partially or completely lie in the range of low Re numbers.

The low Reynolds flows ($10^4 \sim 10^5$) have gradual laminar-turbulent transition and under favorable conditions might appear a laminar separation bubble (LSB) on the surface where separated stream encloses a region of stagnant and reverse flow. In Figure 1 is shown self-explanatory sketch of a laminar separation bubble. Such flows have a complex three-dimensional unsteady nature. Strength, position and extent of the LSB depends on many factors, among the most influential belong the Reynolds number, angle of attack or external factors such as a free-stream turbulence intensity, vortical and acoustic disturbances. Higher angle of attack or Reynolds number usually shortens the length of the bubble (Figure 2).

Moreover, shorter bubbles are more sensitive for sudden changes of velocity or angle of attack

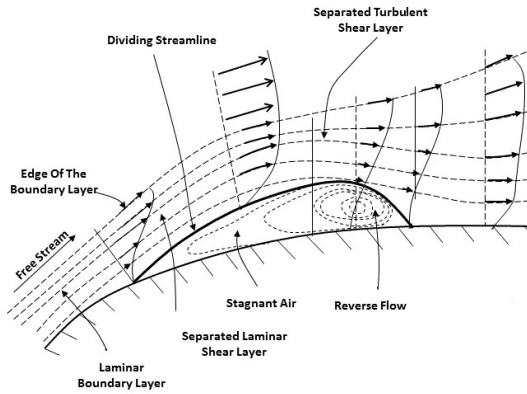


Fig. 1 Nature of laminar separation bubble

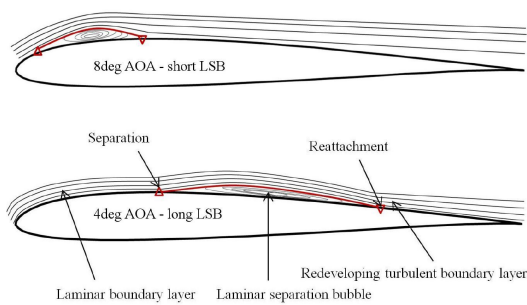


Fig. 2 Short & long laminar separation bubble

which can cause that the shear layer may fail to reattach and it may “burst” to form either a long bubble or an unattached free shear layer.[1]

The initial stage of natural transition is an amplification of acoustic or vortical perturbations of tiny scale within the boundary-layer. The acoustic perturbations tends to influence the growth of two-dimensional instabilities, whereas the vortical perturbations influence the growth of three-dimensional instabilities. Low-order numerical schemes (order of accuracy < 2) with their higher numerical dispersion and dissipation struggle with predictions of complex unsteady flows where ability to resolve small scales of the flow in detail is required. In order to achieve required precision with low-order numerical schemes for flows where demands on accurate results are emphasized, e.g. in aeroacoustics, a tremendous grid resolution would be required which would lead to an unacceptable computational cost. High-order accurate numerical schemes (order of accuracy > 2) have lower numerical dispersion and dissipation and

despite the fact that they are more costly per iteration than low-order methods, one can obtain very accurate results with much lower computational cost than it would be possible with common low-order methods. Among disadvantages of high-order accurate numerical schemes belong that they are often more complicated and still less robust than their low-order counterparts.

The discontinuous Galerkin (DG) method is a major high-order scheme based on weak formulation of conservation laws. Strong mathematical formulation makes its implementation sometimes cumbersome. Concurrently, methods as staggered-grid multi-domain spectral method[2, 3], the spectral difference (SD)[4, 5] and the flux reconstruction (FR)[6, 7] have been subject of research. Those high-order schemes are based on differential form of the governing equations. Differential formulation leads to simpler algorithm with lower computational cost due to absence of numerical integrations. The FR scheme is a high-order accurate conservative scheme proposed by H. T. Huynh in 2007. It uses differential form of Euler or Navier-Stokes equations and it is considered to be more general formulation because it involves only one grid and do not staggers solution and flux points into two grids as staggered-grid spectral method or spectral difference method. It has been found by Huynh that there exist relations between the FR, the DG and the SD method and their simplified equivalents can be recovered within the FR framework. In the previous work on the FR scheme conducted by one of the authors, the vortical flow simulations exhibited a high-resolution property for large-scale vortices in a practical application.[8]

Numerical simulations presented in this paper aims to investigate use of a high-order accurate flux reconstruction (FR) scheme for accurate three-dimensional simulations of transitional flow with small (grid-scale) vortices. Transitional flow over a rectangular wing section with Selig/Donovan low-Reynolds number airfoil has been chosen since it has been subject of several numerical studies. [9, 11, 12, 13, 14]

This introduction section describes the motivation for the current effort. In the second section of this paper, numerical algorithm is briefly pre-

sented. A careful evaluation of numerical simulation results is presented in the third section. Finally, this paper is closed with conclusions and remarks obtained from the current effort.

2 Numerical algorithm

Numerical simulations are carried out on hexahedral domains by a high-order accurate parallel code which solves the unsteady, three-dimensional, compressible Navier-Stokes equations using the FR scheme for spatial discretization. High-order method adds internal solution points (also called degrees of freedom, abbr. DOF) inside each computational cell. The solution polynomial is reconstructed in the cell to achieve high-order accuracy. This concept is well known and shared with other high-order methods including the DG, spectral finite volume (SV) method, SD and FR scheme.

2.1 Formulation of the flux reconstruction scheme

The FR scheme used in this paper was proposed by H. T. Huynh [6, 7] in 2007 and is briefly reviewed in this section. More detailed description can be found in authors' previous work [10] or in Huynh's papers [6, 7] where can be found thorough mathematical explanation.

The conservation form of Navier-Stokes equations is expressed by the following equation,

$$\frac{\partial Q}{\partial t} + \frac{\partial E}{\partial x} + \frac{\partial F}{\partial y} + \frac{\partial G}{\partial z} = 0, \quad (1)$$

where t is time, Q is a vector of conservative variables and E, F and G are flux vectors including inviscid and viscous terms. Computational domain is discretized into non-overlapping hexahedral cells. In each single cell is solution approximated by N pieces of data in all coordinate directions. N pieces of data are solution points, sometimes called degrees of freedom (DOF).

To be able to reconstruct solution within each cell with a polynomial of degree ($p = N - 1$), one need to specify N solution points. Several choices how to define solution points (SP) are available e.g. equidistant, Lobatto or Gauss points etc. (see Figure 2.1)

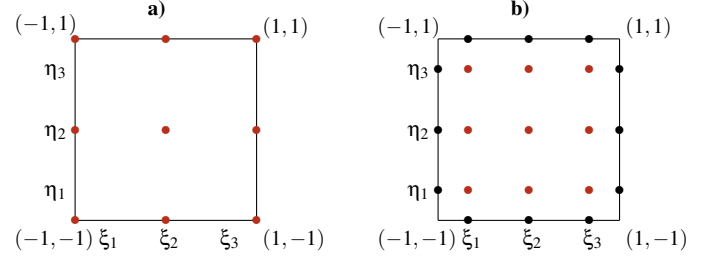


Fig. 3 Solution points on 2D element ($p = 2$) a) Lobatto points (red), some of them lie on the cell edges b) Gauss points (red) are all inside the cell. Black dots show flux points.

Solution can be reconstructed using the tensor product of three 1D Lagrange polynomials of degree $p = N - 1$, thus, solution is reconstructed with N^3 solution points in the cell. In similar fashion are obtained flux polynomials from the flux values at solution points. The flux polynomials are of degree $N - 1$ and they are generally discontinuous across cell interfaces as illustrated in Figure 4. To prevent any loss of information between adjacent cells, the flux polynomials are corrected to have common values at the cell-cell interfaces. Common numerical fluxes are evaluated at each interface using a simple Rusanov scheme (Figure 5 a). The corrected (one can say continuous) flux polynomial should be close to its original and corrected flux polynomial should be N^{th} -order polynomial which ensures that its spatial derivative is of degree $N - 1$, the same degree as of solution polynomial. (Figure 5 b,c) Moreover, the flux derivatives need to be also corrected in a similar manner.

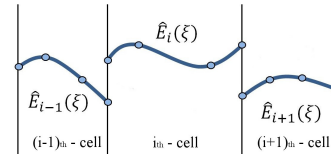


Fig. 4 Flux polynomials are generally discontinuous at the cell-cell interface.

Huynh proposed method using correction functions to modify, one can say 'correct' flux polynomials. Correction functions are of such convenient shape that when added to the polynomial, this polynomial remains close to its original and is modified on the left and right side to

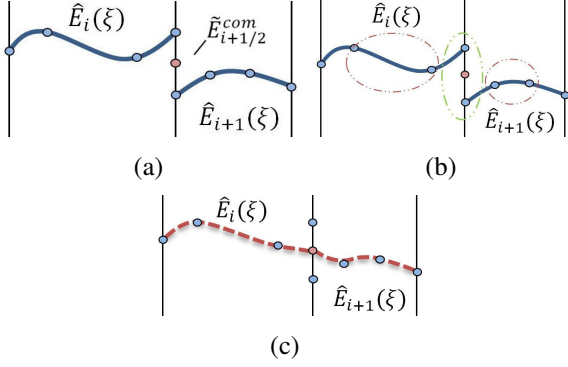


Fig. 5 Flux polynomials are generally discontinuous at the cell-cell interface and they need to be corrected to share same value at the interface.

share common value with the neighboring cell. The correction function, which is a N -order polynomial requires additional $N - 1$ conditions together with prescribed boundary conditions

$$\begin{aligned} g_L(-1) &= 1, & g_L(1) &= 0 \\ g_R(-1) &= 0, & g_R(1) &= 1 \end{aligned} \quad (2)$$

where L and R mean left and right correction function. Huynh derived various correction functions which can be employed, e.g. based on the Legendre, Radau, or Lobatto polynomials. Figure 6 shows three possible “left” correction functions g_L for $N = 4$, ($p = 3$). It has been observed

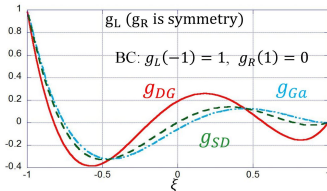


Fig. 6 Correction functions for the flux polynomial. ($p=3$) Only g_L 's are shown due to symmetry.

by Huynh that choice of the correction function has an influence on the stability and accuracy of the scheme. In this study, the correction function is based on the Radau polynomial and scheme exhibits higher accuracy with lower CFL stability as a trade off. The numerical scheme corresponds to the discontinuous Galerkin method. Gauss points are chosen as solution points in this study.

For discretization of the viscous fluxes, the second Bassi-Rebay (BR2) [15] scheme with

compact stencil is implemented and the common viscous fluxes can be easily calculated by the average (centered formula). When inviscid and viscous flux vectors are evaluated at all solution points, one can proceed to evaluate all divergence terms in (1) and update the solution Q in time via a suitable temporal discretization. A non-linear LU-SGS [16] implicit time-integration scheme which was extended to be second order accurate in time has been used in this study.

3 Results and discussion

Simulation results are presented and discussed in the current section. For the purpose of comparison are representatives of various high-order numerical schemes, namely, discontinuous Galerkin and compact differencing scheme chosen. Selected simulations for comparison were conducted by Galbraith & Visbal [12] ($\alpha = 4^\circ$ & 8°), Garmann & Visbal [13] ($\alpha = 8^\circ$). Above mentioned authors have used the 6th-order accurate compact differencing scheme. Simulations using the 4th-order accurate discontinuous Galerkin method have been conducted by Carton de Wiart & Hillewaert [11] ($\alpha = 4^\circ$).

3.1 Numerical setup

Unsteady three-dimensional computations were performed using the flux reconstruction for spatial discretization (second, third and fourth-order of accuracy in space) and implicit lower-upper symmetric Gauss-Seidel (LU-SGS) method for the temporal discretization (second order of accuracy in time).

Simulations are carried out with flow conditions as follows, $Re = 60,000$, free-stream Mach number $M_\infty = 0.1$, constant ratio of specific heats $\gamma = 1.4$ and Prandtl number $Pr = 0.72$.

The Selig-Donovan SD7003 airfoil has a maximum thickness of 8.5% and maximum camber of 1.45% at the 35% chord location. The wing section is created from the extended planar airfoil geometry with spanwise length set to $z/c = 0.2$, see Figure 7.

Two computational domains consist of 16,000 and 32,000 hexahedral cells correspond-

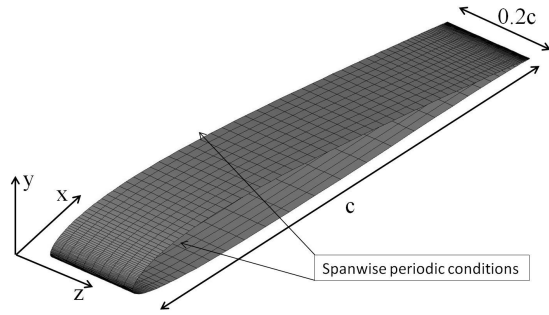


Fig. 7 Selig/Donovan SD7003 low-Reynolds number airfoil

ing in approximately 2,000,000 degrees of freedom at the maximum. An O-grid is surrounding the model with a resolved near-wall layer ($y^+ \approx 1$) and with the far-field boundary condition (free-stream velocity condition) located 100 chords from the model, see Table 1 and Figure 8. On the wing surface is applied a no-slip isothermal condition with a temperature ratio $T_{wall}/T_{inf} = 1.002$ and flow is considered to be periodic in space, thus periodic boundary is applied along the spanwise direction.

Table 1 Computational domains

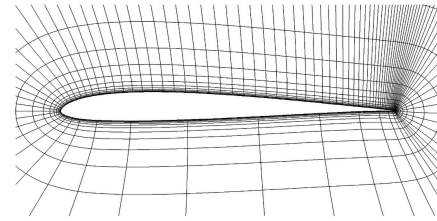
Mesh	Dimensions [†]	Cells	DOF [10 ⁶]		
			2nd	3rd*	4th*
Grid 1	8 × 97 × 25	16,128	0.13	0.43	1.03
Grid 2	8 × 193 × 25	32,256	0.26	0.87	2.06
Grid 3	15 × 193 × 49	129,024	1.03	---	---
Grid 2	at $x/c = 0.6$	x^+	y^+	z^+	
	3rd	17.1	1.35	53	
	4th	11.4	0.9	35	

* Number of solution points per cell is N^3 , where N is the order of accuracy of the scheme.

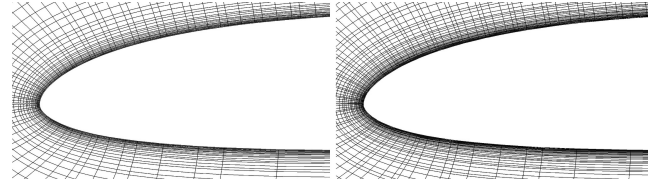
[†] spanwise × circumferential × wall-normal
 y^+ (wall-normal), z^+ (spanwise)

Non-dimensional time steps ($\Delta t^* = \Delta t \times U_\infty/c$) were of the order 10^{-4} . Third-order simulations have been running over a non-dimensional time (N/T) interval of 50 with all quantities of interest averaged during the last N/T interval of 20. To reduce necessary computational time for the fourth-order simulations, an initial flow-field was extrapolated from the third-order simulations using of Lagrange interpolation polynomials.

Averaged flow fields of fourth-order simulations were obtained after letting the flow to sta-



(a) O-grid domain (grid 1)



(b) Solution points, left 3rd (27 points per hexa cell) and right 4th-order (64 points per hexa cell)

Fig. 8 Representation of computational domain

bilize. After that, time averaged data were collected over N/T interval of 10. Figure 9 shows time history of lift and drag coefficient for $\alpha = 4^\circ$ and both computational domains.

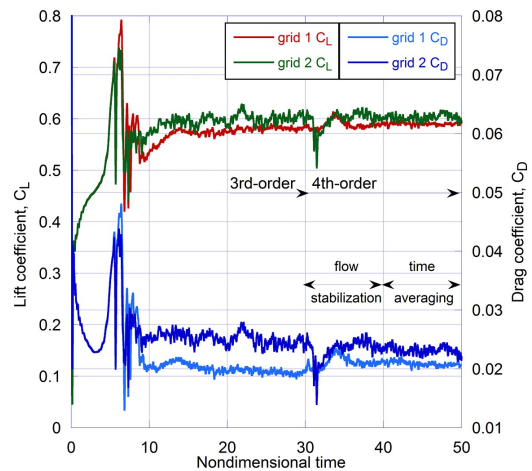


Fig. 9 Time history of C_L and C_D , 4th-order ($p=3$), $\alpha = 4^\circ$

3.2 Angle of attack $\alpha = 4^\circ$

For the sake of clarity and completeness, authors would like to show some results for an angle of attack $\alpha = 4^\circ$ obtained earlier this year. Therefore, an extent of the part for an angle $\alpha = 4^\circ$ is rather limited and more thorough discussion can be found in [10].

At $\alpha = 4^\circ$, a laminar separation bubble on the upper surface of the wing can be characterized in time mean sense as a long and stable. The flow tends to separate from the surface around 20% and reattach back to the surface around 60% of the chord. The mean separation bubble is clearly visible in Figure 11 b). For qualitative comparison are three-dimensional coherent vortices visualized by the iso-surfaces of Q-criterion in Figure 10. Averaged pressure and skin friction coefficient distributions are plotted in Figure 12. Computed boundary-layer profiles of streamwise velocity and Reynolds stress component $\overline{u'^2}$ on grid 2 for the fourth order are compared with profiles obtained from the literature in Figure 13. The profiles of mean-square fluctuations of u-velocity calculated on grid 1 seem to be under-predicted, whereas the grid-2 shows an improvement. With higher grid resolution, especially in streamwise (circumferential) direction, the three-dimensional vortical structures are captured better and the laminar separation bubble and aerodynamic forces reasonable agree with the literature. In Table 2 are summarized time averaged data along with results from the literature for comparison. Obtained results for an angle of attack 4° agree well with the literature despite of use of relatively coarse domains with maximum at 2,000,000 degrees of freedom.

3.3 Angle of attack $\alpha = 8^\circ$

In the following section are presented results for an angle of attack $\alpha = 8^\circ$. Apart of an angle of attack, the numerical setup is without change in parameters. For an angle of attack $\alpha = 8^\circ$ is characteristic that separation occurs almost immediately and flow reattaches at about quarter chord. The laminar bubble is shorter (in time-mean sense) and shifted closer to the leading edge of the wing

(compare Figure 11 and Figure 18). Turbulent flow is over larger part of the wing as shown in Figure 14 of instantaneous Q-criterion iso-surfaces for three orders of accuracy (2^{nd} , 3^{rd} and 4^{th}). Second-order simulation (Figure 14a) with around 130,000 degrees-of-freedom (8 SP per computational cell) is not capable of capturing the three-dimensional breakdown. A robust vortex is periodically formed but because its breakdown is suppressed due to the insufficient grid resolution, the vortex travels further downstream to the trailing edge. Similar behavior has been observed in two-dimensional simulations conducted by the authors earlier. This strong vortex negatively affects flow downstream on the suction side of the wing. The third-order simulation (Figure 14b) with around 430,000 degrees-of-freedom (27 SP per computational cell) shows improving trend since the vortex roll-up and breakdown is more clear without “two-dimensional” effects reported above. Significant change can be seen in Figure 14c) which depicts the fourth-order simulation with around 1,000,000 degrees-of-freedom (64 SP per computational cell). Spanwise vortex is formed and almost immediately decays. For the purpose of evaluation of the effects of order of polynomials, second-order simulation has been computed on grid 3. This domain consists of 129,024 cells and with the second-order code, number of solution points in spanwise, circumferential and normal directions ($28 \times 385 \times 97$) are the same as in the 4th-order simulation, thus, second-order simulation on grid 3 also has 1,000,000 degrees-of-freedom. In (Figure 14c) can be found comparison of both simulations with 1,000,000 DOF's. Second-order simulation shows much worse performance in predicting of three-dimensional vortical structures than its 4th-order counterpart. The vortical structures are similar with the third-order simulation showed in Figure 14b with only approx. 430,000 DOF's. Computational cost of the second-order simulation were somewhere between the computational cost of 4th-order and 3rd-order simulation, thus, it is possible to conclude that the mesh refinement is an inefficient means for low order methods to reach an accuracy threshold. Figure 15 shows time-mean pres-

sure C_p and skin friction C_f coefficient distributions compared with the literature.

The fourth-order simulation with (1,000,000 DOF) seems to be in better agreement with results of Garmann et al. on domain comprising 12,549,120 points than with results obtained by Galbraith et al. on domain consisting of 5,700,000 points. Skin friction coefficient distribution reasonably follows the one by Garmann et al. with drop in friction profile predicted at the same location with the same magnitude. Some discrepancy in the pressure coefficient distribution can be found upstream the turbulent transition. Figure 16a shows comparison of mean boundary-layer streamwise velocity profiles for the fourth-order. Computed boundary layer profiles reasonably follows the profiles of Garmann et al. with velocity slightly overpredicted along the whole suction side of the wing. Reynolds stress component $\overline{u'^2}$ profiles for the fourth order are compared with profiles obtained from the literature in Figure 16b. Even though the grid 1 has lower resolution, magnitude and shape of mean-squared velocity profiles reasonable agree with profiles from the literature with some discrepancies which are clearly visible in the most sensitive area of transition to turbulence at $x/c = 0.2$ and $x/c = 0.3$. Table 3 contains summary of time-mean results and summary of results from the literature.

The comparison of average pressure coefficient and skin friction coefficient on the airfoil obtained with the second, third and fourth-order simulations can be seen in Figure 17. Second-order simulation with 130,000 DOF's shows poor results due to the "two-dimensional" effect reported earlier. The third-order simulation predicts location of the turbulent transition more upstream. The same behavior has been observed for an angle of attack $\alpha = 4^\circ$ where resolution of this domain has been classified as an insufficient. Second-order simulation with 1,000,000 DOF's also shows poor results in comparison with the 4th-order case with 1,000,000 DOF's. Separation and transition to turbulence is predicted better than in the 3rd-order simulation and distribution reasonable follows the 4th-order distribution until the transition point (approx. at $x/c = 0.2$).

After the transition to turbulence, are forces significantly different. It can be seen that pressure gradient in C_p plot is not so steep (from $x/c = 0.2$ to $x/c = 0.4$), drop in friction profile is wider and friction profile is not recovered properly at the rear part of the wing which may indicate that the vortex breakdown is slower and its disintegration is over larger portion of the wing. Further analysis of the results will be presented at the conference.

Contours of turbulent kinetic energy T.K.E. for all simulations are shown in Figure 19. Figure 20 shows contours of turbulent kinetic energy computed on the fine domain with 12.5 MDOF's by Garmann et al. Fourth-order results agree well and are consistent with the literature. The slight difference in T.K.E magnitude can be attributed to the effects of fairly coarse grid resolution consisting of 1,000,000 degrees of freedom.

4 Conclusion

This paper presents some preliminary results obtained with the flux reconstruction scheme for the prediction of transition associated with a laminar separation bubble on the SD7003 airfoil. Simulations are performed using second, third and fourth order accurate code. The grid resolution of the second and third order simulations is too coarse for the small energetic scales to be well captured, nevertheless, fourth-order simulation shows a remarkable agreement with results obtained with much finer LES simulation [13].

5 Acknowledgments

One of the authors, V. Skarolek gratefully acknowledge the support of Japanese Government through a Monbukagakusho:MEXT(Ministry of Education, Culture, Sports, Science and Technology) scholarship.

References

- [1] Gaster M. The Structure and Behaviour of Laminar Separation Bubbles. *Reports and memoranda no.3595*, Aerodynamics Division N.P.P., London, 1967
- [2] Kopriva D.A, Kalias J.H. A Conservative Staggered-Grid Chebyshev Multidomain Method for Compressible Flows. *Journal of Computational Physics*, Vol. 125, pp 244-261, 1996.
- [3] Kopriva D.A. A Staggered-Grid Multidomain Spectral Method for the Compressible Navier Stokes Equations. *Journal of Computational Physics*, Vol. 143, pp 125-158, 1998.
- [4] Liu Y, Vinokur M, Wang Z.J. Multi-dimensional Spectral Difference Method for Unstructured Grids. *40th AIAA Aerospace Sciences Meeting and Exhibit*, AIAA 2005-0320, 2005.
- [5] Liu Y, Vinokur M, Wang Z.J. Spectral Difference Method for Unstructured Grids I: Basic formulation. *Journal of Computational Physics*, Vol. 216, pp 780-801, 2006.
- [6] Huynh H.T. A Flux Reconstruction Approach to High-Order Schemes Including Discontinuous Galerkin Methods. *18th AIAA Computational Fluid Dynamics Conference*, AIAA 2007-4079, 2007.
- [7] Huynh H.T. A Reconstruction Approach to High-Order Schemes Including Discontinuous Galerkin for Diffusion. *47th AIAA Aerospace Sciences Meeting Including The New Horizons Forum and Aerospace Exposition*, AIAA 2009-403, 2009.
- [8] Miyaji K. Vortical flow simulations by a high-order accurate unstructured hexahedral grid method. *Comput Fluids*, 2012.
- [9] Uranga A, Persson P.-O, Drela M, Peraire J. Implicit Large Eddy Simulation of Transitional Flows Over Airfoils and Wings. *19th AIAA Computational Fluid Dynamics*, AIAA 2009-4131, 2009.
- [10] Skarolek V, Miyaji K. Transitional Flow over a SD7003 Wing Using Flux Reconstruction Scheme. *52nd Aerospace sciences meeting*, AIAA 2014-0250, 2014.
- [11] Carton de Wiart C, Hillewaert K. DNS and ILES of transitional flows around a SD7003 using a high order Discontinuous Galerkin method. *Seventh International Conference on Computational Fluid Dynamics*, ICCFD7-3604, 2012.
- [12] Galbraith M, Visbal M.R. Implicit Large Eddy Simulation of Low Reynolds Number Flow Past the SD7003 Airfoil. *40th Fluid Dynamics Conference and Exhibit*, AIAA-2010-4737, 2010.
- [13] Garmann D.J, Visbal M.R, Orkwis P.D. Comparative study of implicit and subgrid-scale model large-eddy simulation techniques for low-Reynolds number airfoil applications. *Int. J. Numer. Meth. Fluids*, 71:1546-1565, 2012.
- [14] Zhou Y, Wang Z.J. Implicit Large Eddy Simulation of Transitional Flow over a SD7003 Wing Using High-Order Spectral Difference Method. *40th Fluid Dynamics Conference and Exhibit*, AIAA 2010-4442, 2010.
- [15] Bassi F, Rebay S. A High-Order Accurate Discontinuous Finite Element Method for the Numerical Solution of the Compressible Navier-Stokes Equations. *Journal of Computational Physics* 131, 267-279, 1997.
- [16] Sun Y, Wang Z.J, Liu Y. Efficient Implicit Non-linear LU-SGS Approach for Compressible Flow Computation Using High-Order Spectral Difference Method. *Communications in Computational Physics*, vol. 5, 760-778, 2009.

Copyright Statement

The authors confirm that they, and/or their company or organization, hold copyright on all of the original material included in this paper. The authors also confirm that they have obtained permission, from the copyright holder of any third party material included in this paper, to publish it as part of their paper. The authors confirm that they give permission, or have obtained permission from the copyright holder of this paper, for the publication and distribution of this paper as part of the ICAS 2014 proceedings or as individual off-prints from the proceedings.

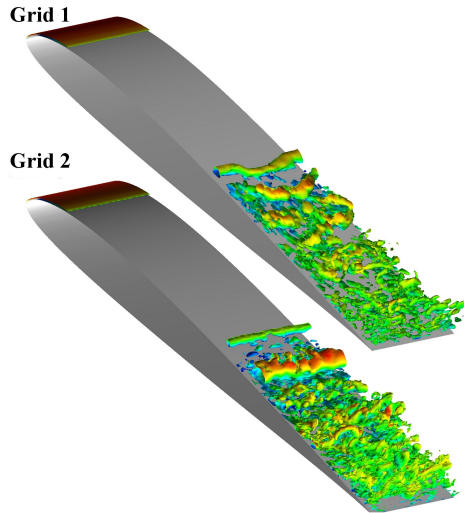
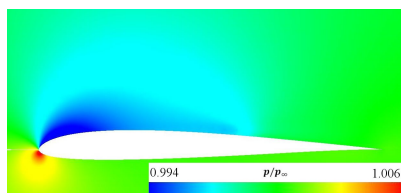


Fig. 10 Instantaneous iso-surface of Q-criterion (4th-order, $\alpha = 4^\circ$, $Q=500$, colored by Mach number)

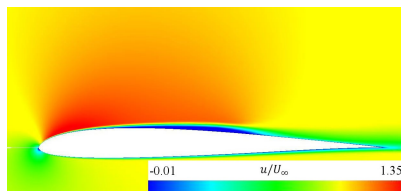
Table 2 : $\alpha = 4^\circ$ Time averaged results: present study and literature.

Source	N	x_{sep}/c	x_r/c	$\overline{C_L}$	$\overline{C_D}$	DOF
Simulations						$[10^6]$
(CD) Galbraith	6	0.23	0.65	0.59	0.021	5.7
(CD) Galbraith	6	0.20	0.66	-	-	6.6
(DG) Carton de Wiart	4	0.207	0.647	0.607	0.0201	0.8
(DG) Carton de Wiart	4	0.209	0.654	0.602	0.0196	11
Present study						
(FR) Grid 1	3	0.237	0.626	0.5887	0.0191	0.4
(FR) Grid 1	4	0.224	0.646	0.5902	0.0208	1.0
(FR) Grid 2	3	0.203	0.662	0.6035	0.0215	0.9
(FR) Grid 2	4	0.201	0.657	0.5987	0.0221	2.0

N - order of accuracy, x_{sep} - separation, x_r - reattachment
 CD - compact differencing scheme, DG - discontinuous Galerkin, FR - flux reconstruction

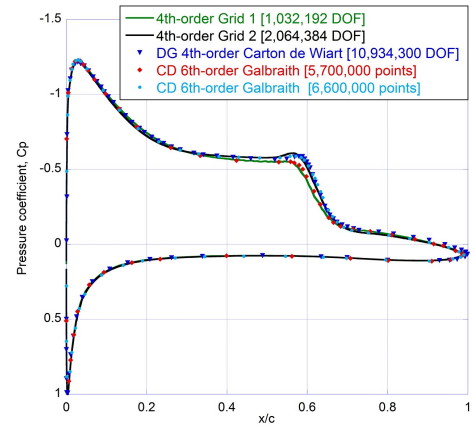


(a) 4th-order, grid 1, pressure

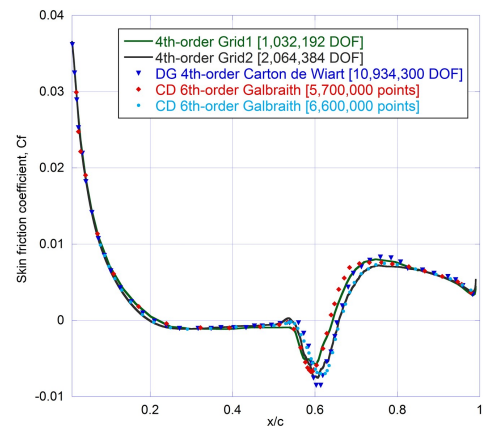


(b) 4th-order, grid 1, u-velocity

Fig. 11 Pressure and u-velocity contours for $\alpha = 4^\circ$.

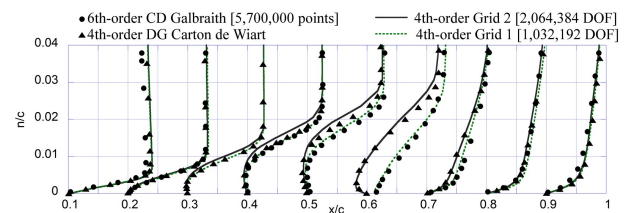


(a) C_p

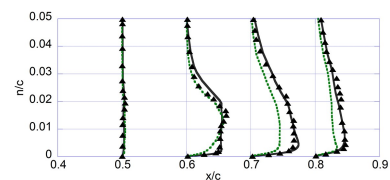


(b) C_f

Fig. 12 Comparison of mean (a) C_p and (b) C_f distributions with the literature at $\alpha = 4^\circ$.



(a) u-velocity



(b) $\overline{u'^2}$

Fig. 13 Boundary layer profiles of (a) u-velocity (b) mean-squared fluctuations of u-velocity (u'^2) at $\alpha = 4^\circ$.

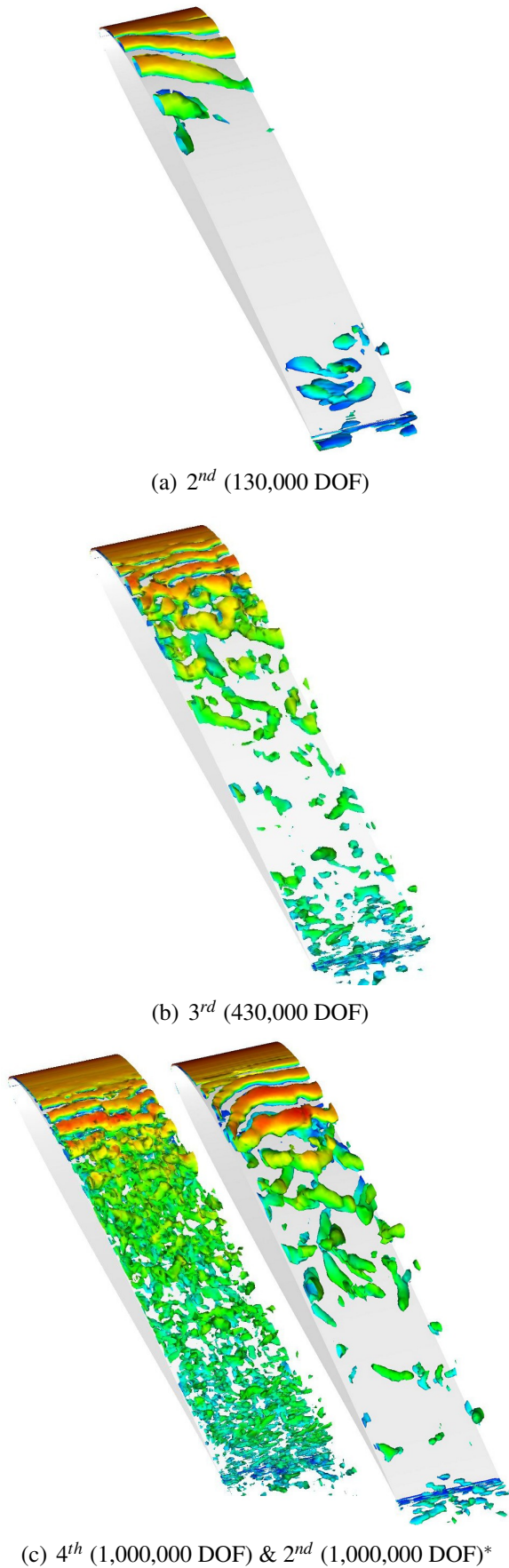
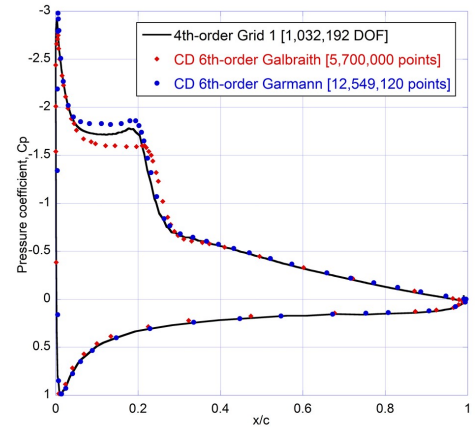
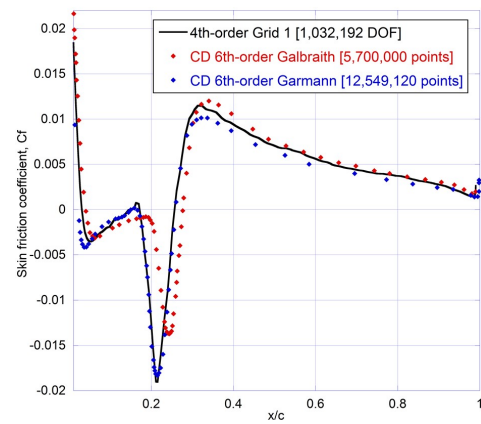


Fig. 14 Grid 1: Instantaneous iso-surface of Q-criterion ($\alpha = 8^\circ$, $Q=300$, colored by Mach number), ad a) * Grid 3

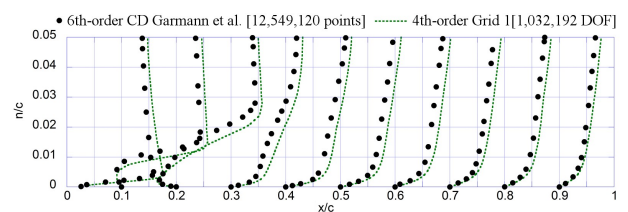


(a) C_p

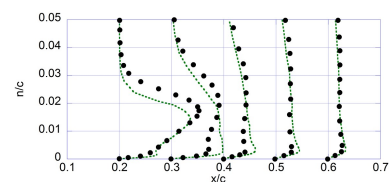


(b) C_f

Fig. 15 Comparison of mean (a) C_p and (b) C_f distributions with the literature at $\alpha = 8^\circ$.



(a) u-velocity



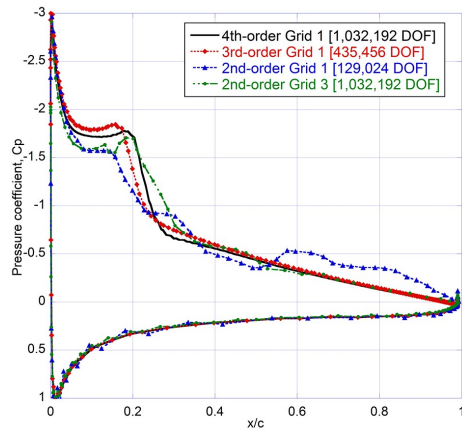
(b) $\overline{u'^2}$

Fig. 16 Boundary layer profiles of (a) u-velocity (b) mean-squared fluctuations of u-velocity ($\overline{u'^2}$) at $\alpha = 8^\circ$.

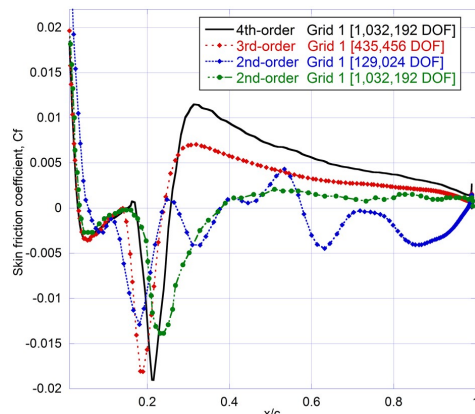
Table 3 : $\alpha = 8^\circ$ Time averaged results: present study and literature.

Source		x_{sep}/c	x_r/c	$\overline{C_L}$	$\overline{C_D}$	DOF
Simulations	N					$[10^6]$
(CD) Galbraith et al.	6	0.04	0.28	0.92	0.043	5.7
(CD) Garmann et al.	6	0.023	0.259	0.9696	0.0391	12.5
Present study						
(FR) Grid 1	3	0.031	0.24	0.9545	0.0349	0.4
(FR) Grid 1	4	0.028	0.257	0.9331	0.0389	1.0

N - order of accuracy, x_{sep} - separation, x_r - reattachment
 CD - compact differencing scheme, FR - flux reconstruction

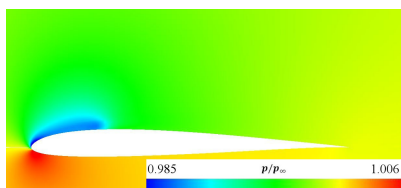


(a) C_p

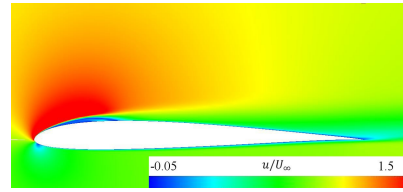


(b) C_f

Fig. 17 Mean (a) C_p and (b) C_f distributions for various orders of accuracy at $\alpha = 8^\circ$.

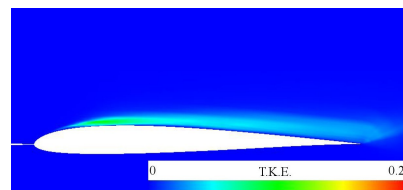


(a) pressure

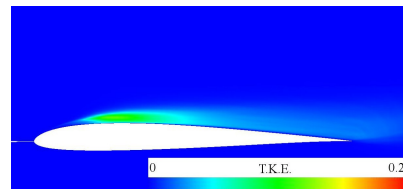


(b) u-velocity

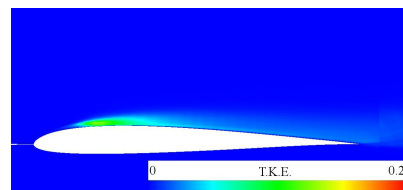
Fig. 18 Contours for $\alpha = 8^\circ$. (4th-order, grid 1)



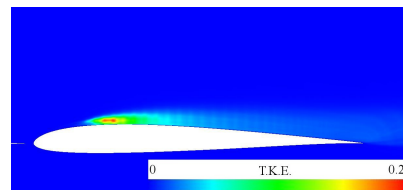
(a) 2nd-order, grid 1, T.K.E



(b) 2nd-order, grid 3, T.K.E

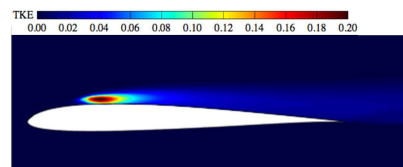


(c) 3rd-order, grid 1, T.K.E



(d) 4th-order, grid 1, T.K.E

Fig. 19 Turbulent kinetic energy contours for $\alpha = 8^\circ$.



(a) T.K.E

Fig. 20 Previous result of Garmann et al.[13] at $Re = 60000$, $\alpha = 8^\circ$.